

Evidence for surface cooling emission in the XMM-Newton spectrum of the X-ray pulsar PSR B2334+61

K.E. McGowan^{1,2}, S. Zane¹, M. Cropper¹, W.T. Vestrand², F.A. Córdova³, C. Ho²

km2@mssl.ucl.ac.uk

ABSTRACT

We report on the first *XMM-Newton* observation of the Vela-like pulsar PSR B2334+61. Spectral analysis reveals soft X-ray emission, with the bulk of the photons emitted at energies below ~ 1.5 keV. We find that the spectrum has a thermal origin and is well-fitted with either a blackbody or a magnetized, pure H atmospheric model. In the latter case, for a neutron star with a radius of 13 km and a magnetic field of 10^{13} G, the best-fit gives an hydrogen column density $N_H = 0.33 \times 10^{22}$ cm⁻² and an effective temperature $T_{eff}^\infty = 0.65 \times 10^6$ K, as measured at Earth. A comparison of the surface temperature of PSR B2334+61 obtained from this fit with cooling curves favor a medium mass neutron star with $M \sim 1.45M_\odot$ or $M \sim 1.6M_\odot$, depending on two different models of proton superfluidity in the interior. We do not detect any pulsed emission from the source, and determine an upper limit of 5% for the modulation amplitude of the emission on the pulsar's radio frequency.

Subject headings: pulsars: individual (PSR B2334+61) — stars: neutron — X-rays: stars

1. Introduction

Young pulsars, neutron stars in supernova remnants (SNRs) and cooling neutron stars are among the wider classes of radio-pulsars which can be detectable at higher energies, i.e. in the optical, X-ray and gamma-ray bands. Observations at these wavelengths are central

¹Mullard Space Science Laboratory, University College of London, UK

²Los Alamos National Laboratory, Los Alamos, NM 87545

³Chancellor's Office, University of California, Riverside, CA 92521

to understanding the pulsar physics since it is only at these energies that both the central neutron star and the surrounding nebula become observable.

X-ray radiation detected from rotation-driven pulsars has to be attributed to a blend of various thermal and non-thermal emission processes (e.g. Becker & Aschenbach 2002):

- non-thermal emission from charged relativistic particles accelerated in the pulsar magnetosphere. This emission is characterized by power-law like spectra over a broad energy band from the optical to the gamma-ray band;
- extended non-thermal emission from the pulsar-driven synchrotron nebula. Depending on the local conditions (e.g. matter density in the ambient medium) it can be observed from radio through hard X-ray energies;
- emission from heated polar caps, which can have either a thermal or non thermal character;
- photospheric emission from the surface of a cooling neutron star. In this case a modified blackbody spectrum and a low amplitude intensity variation are expected, observable from the optical to the soft X-ray range depending on the neutron star age.

In pulsars older than 10^6 yr standard cooling scenarios predict a sharp reduction in the surface temperature when surface photon emission overtakes the neutrino luminosity losses (Nomoto & Tsuruta 1987), while in pulsars younger than 10^4 yr strong magnetospheric emission swamps the weaker thermal radiation. The non-thermal component in X-ray emission of middle-aged pulsars (ages $10^4 - 10^6$ yr) is much fainter, and the thermal radiation from the neutron star surface ($T \sim 0.02 - 0.1$ keV) can dominate at soft X-ray/UV energies. Soft X-ray observations of the photon flux emitted from the surface of neutron stars confronted with calculations of their thermal evolution provide one of the most useful diagnostics of the physical processes operating in the dense interiors of such stars (Schaab et al. 1999).

Although X-ray observatories like *ROSAT*, *ASCA*, *BeppoSax* and *RXTE* have made important progress in neutron star and pulsar astronomy, the quality of the data obtained in the past with different instruments and/or in different wavebands is inevitably rather inhomogeneous, and with low S/N ratios. The conclusions drawn on these data are therefore unlikely to be firm in a number of cases: for many of the X-ray detected objects only a marginal detection is available, and the low number of total counts is insufficient to make a spectral (not to mention timing) analysis. In addition to other things, this prevents a discrimination between the emission scenarios described above. The advent of satellites such as *XMM-Newton*, which has a large collecting area, permits the observation of very faint

sources not previously accessible. Even for very faint and distant objects, like that presented in this paper, we can now discriminate whether the dominant mechanism is thermal or non-thermal which in turn permits the first estimates of temperature and/or power law index. The former, in particular, is essential to localize the X-ray emitting pulsar in the thermal and evolutionary diagram, with the ultimate goal to provide the first observational constraints on the equation of state of matter at supra-nuclear densities. At present, only a very low number of sources are available for this exercise, therefore any new source in the plot is important.

PSR B2334+61 is a Vela-like pulsar located at a distance of $D = 3.1_{-1.0}^{+0.2}$ kpc (Cordes & Lazio 2002) and associated with the supernova remnant (SNR) G114.3. With a spin-down age of $\sim 4 \times 10^4$ yr it is one of the oldest pulsars which is still associated with a SNR. It has a spin period of $P = 0.495$ s, considerably larger with respect to the other SNR-associated pulsars, and a large spin-down rate, $\dot{P} = 191 \times 10^{-15}$ s s $^{-1}$, which in turn implies a magnetic field of $B \sim 10^{13}$ G. PSR B2334+61 was originally detected in a short (8 ks) *ROSAT* pointing (Becker et al. 1996) but the small number of counts precluded any detailed spectral analysis or testing for modulations. Here we report on the first *XMM-Newton* observation of the source.

2. Observations and data reduction

PSR B2334+61 was observed with *XMM-Newton* on 2004 February 12. For the spectral and timing analysis we used data from the European Photon Imaging Camera (EPIC) instruments: the EPIC MOS detector (Turner et al. 2001) and the EPIC-PN detector (Strüder et al. 2001). Both MOS instruments and the PN were configured in *full frame* mode and we used the thin filter. The MOS1 and MOS2 observations had total exposure times of 47.5 ks. The EPIC-PN buffer was filled during the observation resulting in an exposure time of 45.8 ks. We reduced the EPIC data with the *XMM-Newton* Science Analysis System (SAS version 6.0.0).

In order to maximize the signal-to-noise ratio for our *XMM-Newton* observation, we filtered the data to include only single, double, triple and quadruple photon events for the MOS, and only single and double photon events for the PN. We included photons with energies only in the range 0.3 – 10 keV.

To verify that there is no contribution to the measured emission from the remnant, we compared the radial profile of the pulsar emission with the *XMM-Newton* point-spread function for EPIC-PN at 1.5 keV, which we generated using the King profile parameters

included in the *XMM-Newton* calibration file "XRT3_XPSF_0006.CCF.plt"¹. We find that the emission we detect from PSR B2334+61 is consistent with that from a point source.

Data have been extracted using a circular region of radius 30", centered on the radio pulsar's position. We obtained 600 counts from MOS1, 616 from MOS2, and 2384 from PN. By using a region of equal size offset from the pulsar's position, we found that the background contributes 439 counts in MOS1, 449 in MOS2, and 1846 in PN. We detect X-rays from PSR B2334+61 at a level of 5σ in MOS1, 5.1σ in MOS2, and 8.3σ in PN. The extraction radius we used encircles 85% of the energy from the source in MOS and 83% in PN. The measured fluxes reported in Table 1 have been corrected accordingly.

3. Spectral Analysis

In order to perform the spectral analysis, we extracted the pulsar spectrum from the MOS1, MOS2 and PN event files. Data were filtered to exclude events that may be incorrect, for example those next to the edges of the CCDs and next to bad pixels. The three spectra were regrouped by requiring at least 50 counts per spectral bin. For each spectrum we created a photon redistribution matrix (RMF) and ancillary region file (ARF). The subsequent spectral fitting and analysis was performed using XSPEC, version 11.3.1.

Since essentially no emission is detected at energies > 1.5 keV, we modeled the MOS spectra over 0.5 – 1.5 keV and the PN spectrum over 0.3 – 1.5 keV (taking into account the calibration uncertainties for the MOS at low energies). We fitted the combined MOS and PN spectra using different models: initially a power-law, a blackbody and a combination of both, each modified by photoelectric absorption (wabs in XSPEC). The best-fit results are summarized in Table 1. The χ^2 values indicate that the spectrum is better represented by a thermal (blackbody) model, rather than by an absorbed power-law. The additional power law component in the third (and fifth) fit is poorly constrained, and not required: by applying an F -test, we find an F -statistic of 1.6 and probability of 0.2. The best-fit blackbody fit gives $N_H = 0.26 \times 10^{22} \text{ cm}^{-2}$ and $T^\infty = 1.62 \times 10^6 \text{ K}$ (where T^∞ is the blackbody temperature measured at Earth²; see Figure 1, first and second panels). We notice that, consistently, this value for the hydrogen column density is lower than the Galactic one in the source direction, which is $N_H \sim 0.84 \times 10^{22} \text{ cm}^{-2}$, while the same argument can only be applied marginally

¹See <http://xmm.vilspa.esa.es/docs/documents/CAL-SRN-0100-0-0.ps.gz> for more information

²We note that T_{eff}^∞ can be obtained by red-shifting at Earth the effective temperature measured at the neutron star surface, T_{eff} , through the relation $T_{eff}^\infty = T_{eff}(1 - 2.952M_{ns}/R)^{0.5}$. T_{eff} is one of the best-fitting parameters of the NSA model.

(within the lower limit of the error bars) to the value of N_H inferred from the power-law fit. The radius of the emitting region, as derived from the blackbody fit using the Cordes & Lazio (2002) distance, is $R_{em} = 1.66^{+0.59}_{-0.39}$ km.

In order to attempt a different representation of the thermal emission detected from PSR B2334+61, we used a magnetized, pure H atmospheric model (nsa in XSPEC, for details see Pavlov et al. 1992 and Zavlin et al. 1996), by fixing the magnetic field at $B = 10^{13}$ G, the value inferred from the radio timing measurements of the source. The neutron star mass and radius (measured at the source) were fixed at $M_{ns} = 1.4M_{\odot}$ and $R = 10$ km, respectively, although the spectral fit is not particularly sensitive to these parameters (see §5 for an a posteriori estimate of the mass). We found that this model also provides an excellent representation of the pulsar spectrum, and the best-fit parameters are $N_H = 0.42 \times 10^{22}$ cm $^{-2}$ and $T_{eff}^{\infty} = 0.58 \times 10^6$ K, where T_{eff}^{∞} is the effective temperature as measured at Earth² (see Table 1). However, this fit gives a pulsar distance of $D = 1.1 \pm 0.6$ kpc, lower than that inferred from the value of the electron density ($D = 3.1^{+0.2}_{-1.0}$ kpc, Cordes & Lazio 2002). Although the pulsar distance and radius are poorly constrained by our data, we find that a better agreement can be reached by using the same atmospheric model and fixing the neutron star radius at a slightly larger value of 13 km. In this case, we find $N_H = 0.33 \times 10^{22}$ cm $^{-2}$ and $T_{eff}^{\infty} = 0.65 \times 10^6$ K (see Table 1 and Figure 1, third and fourth panels). The distance resulting from this fit is $D = 3.2 \pm 1.7$ kpc, which is consistent with the electron density distance. Finally, we verified that even when the thermal component is modeled by a neutron star atmosphere, an additional power law is not required (last fit in Table 1).

We note that the residuals from the model fits shown in Figure 1 are relatively large at $\sim 0.6 - 0.7$ keV. To try and reduce the residuals we fitted the data using the previous models, each modified by an absorption, namely phabs or tbabs in XSPEC. We find that the resulting fits are not improved with respect to our previous results.

4. Timing Analysis

For the timing analysis we only used PN data, extracted by applying the filtering criteria and extraction region previously described in §2; the filtered file was then barycentrically corrected. In order to search for an X-ray modulation at the PSR B2334+61 spin period, we first determined a predicted pulse period at the epoch of our *XMM-Newton* observations, assuming a linear spin-down rate and using the radio measurements (Dewey et al. 1985; Hobbs et al. 2004). We calculate $P = 0.495355469$ s ($f = 2.0187523$ Hz) at the midpoint of our observation (MJD 53,047.6). As glitches and/or deviations from a linear spin-down may alter the period evolution, we then searched for a pulsed signal over a wider frequency range

centered on $f = 2.01875$ Hz. We searched for pulsed emission using two methods. In the first method we implement the Z_n^2 test (Buccheri et al. 1983), with the number of harmonics n being varied from 1 to 5. In the second method we calculate the Rayleigh statistic (de Jager 1991; Mardia 1972) and then calculate the maximum likelihood periodogram (MLP, Zane et al. 2002) using the C statistic (Cash 1979) to determine significant periodicities in the data sets.

We do not find any significant peak near to the predicted frequency with either method, either using the whole 0.3 – 10 keV energy band or restricting the search to the 0.3 – 1.5 keV band. By folding the light curve of PSR B2334+61 on the radio frequency and fitting it with a sinusoid, we determine an upper limit for the pulsation of 5% in modulation amplitude (defined as $(F_{max} - F_{min}) / (F_{max} + F_{min})$ where F_{max} and F_{min} are the maximum and minimum of the pulse light curve).

5. Discussion

We have presented the results from the first *XMM-Newton* observation of PSR B2334+61. The source has been positively detected in all EPIC instruments, although the X-ray emission is very faint and the spectrum does not have a high enough signal-to-noise to make a detailed multi-component fit. However, single component fits allowed us to discriminate between a thermal (blackbody-like) or non-thermal (power law-like) nature of the dominant emission mechanism. We find that the spectrum is well represented by either thermal blackbody-like emission from a small emitting area (e.g. a hot polar cap) of size ~ 2 km or emission from a pure H atmosphere of a neutron star with $R \sim 13$ km and magnetic field $B \sim 10^{13}$ G. The EPIC flux, measured in the 0.3 – 10 keV band, is $(9.2_{-0.9}^{+0.6}) \times 10^{-14}$ erg cm^{-2} s^{-1} and $(1.7_{-1.6}^{+0.1}) \times 10^{-13}$ erg cm^{-2} s^{-1} , in the two cases respectively. Both values are slightly higher than that previously inferred by Becker et al. (1996), $(7.1 \pm 0.2) \times 10^{-14}$ erg cm^{-2} s^{-1} , although we note that due to their limited counts *ROSAT* data could only be analyzed by making an assumption a priori on the spectral shape. In both cases, the value of N_H is consistently lower than the total galactic one in the pulsar direction. A fit with a power-law model alone is statistically worse, and we find little evidence for the presence of a non-thermal component in the spectrum in addition to the thermal one. The upper limit for the flux contribution from the power-law in the energy range 0.3 – 1.5 keV to the blackbody fit is 3%, and to the magnetized atmospheric model fit is $\ll 1\%$. We do not detect X-ray pulsations corresponding to the radio signal, to a limit of 5% in modulation amplitude.

Although both thermal fits are conceivable options, we tend to prefer the atmospheric model representation based on physical grounds. In this case, magnetic effects for a field

strength of order $\sim 10^{13}$ G (which is the value inferred from measurements of the source spin period and period derivative in the radio band) are consistently accounted for in the radiative transfer computation. Moreover, a value for the radius of $\sim 10 - 13$ km is in agreement with the prediction of several neutron star equations of state (Lattimer & Prakash 2001) and we found that this parameter can be successfully adjusted to make the distance inferred from the spectral fit consistent with that obtained from the electron density value of this pulsar.

To date, thermal emission has been detected in only very few radio pulsars: PSR B0656+14 (Possenti et al. 1996), PSR B1055-52 (Pavlov et al. 2002), PSR J0437-4715 (Zavlin et al. 2002), PSR J0538+2817 (McGowan et al. 2003), Geminga (Halpern & Wang 1997), Vela (Pavlov et al. 2001), and PSR B1706-44 (Gotthelf et al. 2002, McGowan et al. 2004). In the case of the first three objects the thermal emission detected above ~ 0.5 keV is more likely to originate from a hot-polar cap. These sources are in fact old pulsars, at a more advanced stage of their cooling history and their surface emission should peak at much lower (UV) energies. This idea was strengthened by the detection of a further thermal component below 0.7 keV (Pavlov et al. 2002) in the spectrum of the brightest of them, PSR B0656+14. The Vela pulsar and PSR B1706-44 are younger ($\tau \sim 10^4$ yrs) and are the only radio active sources for which the thermal component observed in the soft X-rays is well explained by a magnetized cooling atmosphere (Pavlov et al. 2001, McGowan et al. 2004). When this model is assumed instead of a blackbody, the inferred radius is in agreement with a neutron star equation of state. The only other neutron stars whose thermal component is better described by an atmospheric model, and for which this interpretation resolves all the inconsistencies which follow from the blackbody interpretation, are the radio-silent neutron stars 1E 1207-52 (Zavlin et al. 1998) and RX J0822-4300 (Zavlin et al. 1999).

The *XMM-Newton* observation reported here allows us to add another entry to the list. If indeed the X-ray emission detected from PSR B2334+61 is originating in the cooling atmosphere of the neutron star, our estimate of the effective temperature allows us to localize the object in the neutron stars thermal evolutionary diagram.

Our knowledge of neutron star interiors is still uncertain and accurate measurements of the neutron star surface temperature are particularly important to constrain the cooling models and provide information on the physics of the neutron star. Roughly speaking, theoretical models predict a two-fold behavior of the cooling curves depending on the star mass. In low-mass neutron stars neutrino emission is mainly due to a modified Urca process and nucleon-nucleon bremsstrahlung. These are relatively weak mechanisms and produce *slow cooling*. In stars of higher mass the neutrino emission is enhanced by a direct Urca process (or other mechanisms in exotic matter), therefore these stars cool down much faster (*fast cooling* regime). To date (see Yakovlev et al. 2002 for a discussion) it has been realized that

simple models which do not account for proton and neutron superfluidity fail in explaining the surface temperatures observed in many sources, unless objects such as e.g. Vela, Geminga, RX J1856-3754 do have exactly the critical mass that bounds the transition between the very different *slow cooling* and *fast cooling* regimes. This unlikely fine-tuning is not required if the effects of nucleon superfluidity are accounted for. In particular, models with proton superfluidity included predict an intermediate region between fast cooling and slow cooling curves, which is expected to be populated by medium mass neutron stars (roughly with M between 1.4 and 1.65 M_{\odot}). Although the full picture only holds if, at the same time, neutron superfluidity is assumed to be rather weak, it is still interesting that many neutron stars (as 1E 1207-52, Vela, RX J1856-3754, PSR 0656+14) have a surface temperature which falls in such a transition region (Yakovlev et al. 2002). In turn, this means that measuring the surface temperature allows us to “weigh” neutron stars (Kaminker et al. 2001). As we can see from the first two panels of Figure 2 in Yakovlev et al. (2002), assuming an age of $\log \tau = 4.6$, the surface temperature of PSR B2334+61 derived from the blackbody fit is even higher than the upper cooling curves i.e. those corresponding to the slow cooling regime. However, the surface temperature $\log T^{\infty} = 5.9$ obtained by fitting with the magnetized model and $R = 13$ km falls well within the above mentioned transition region of medium mass neutron stars. The mass of PSR B2334+61 should then be $\sim 1.45M_{\odot}$ or $\sim 1.6M_{\odot}$, depending on the kind of proton superfluidity assumed in the model (1p and 2p respectively). Indeed, the measured properties of PSR B2334+61 reported here are in remarkable agreement with that measured for PSR B1706-44 (McGowan et al. 2004).

As mentioned in the introduction, we are now in the position to make the first experimental studies of surface temperatures of isolated neutron stars. However, although most of our insight of neutron star temperatures and interior rely on them, at present these studies have to be considered as pioneering. Only a few sources are currently available for this kind of exercise, so every newly discovered candidate is important. At present, X-ray spectra of thermal emission from NSs are fitted with either a blackbody or magnetic atmosphere models. Although the latter definitely represent a substantial improvement, inasmuch they include most of the relevant physics, a large amount of work remains to be done before they can be claimed to be fully satisfactory. The same is true for the cooling curves: progress has been made in improving these models but they can not yet be considered as completely realistic. Beside other effects we caveat that both, spectra and cooling curves, are computed assuming 1-dimensional transfer of radiation/heat in a single effective temperature, a single magnetic field zone and neglect all effects of more realistic neutron star thermal and magnetic surface distributions (see Zane & Turolla 2005, Page et al. 2004, Blaschke et al. 2004). However, what values to include for these parameters is not necessarily obvious as it is not completely clear what the NS surface temperature distribution is even in the case of a simple

dipolar magnetic field (see Geppert, Küker & Page 2004). We also note that interpreting the temperatures obtained from the spectral fits in the context of theoretical cooling curves relies on the true age of the pulsar being the same as the characteristic spin-down age, which may not be valid. Our results for PSR B2334+61 provide information that helps to constrain the current models and will enable more realistic models to be produced in the future.

This work is based on observations obtained with *XMM-Newton*, an ESA science mission with instruments and contributions directly funded by ESA Member States and NASA. KEM and SZ acknowledge the support of the UK Particle Physics and Astronomy Research Council (PPARC). Part of this work was supported by NASA grant R-2865-04-0. We thank the anonymous referee for a careful reading of the manuscript and several helpful comments.

REFERENCES

- Becker, W., Brazier, K. T. S., Trümper, J. 1996, *A&A*, 306, 464
- Becker, W., Aschenbach, B. 2002, in *Proc. 270 WE-Heraeus Seminar, Neutron Stars, Pulsars, and Supernova Remnants*, ed. W. Becker, H. Lesh, & J. Trümper (Garching bei München: MPI), 273
- Blaschke, d., Grigorian, H., Voskresensky, D.N. 2004, *A&A*, 424, 979
- Buccheri, R., et al. 1983, *A&A*, 128, 245
- Cash, W. 1979, *ApJ*, 228, 939
- Cordes, J. M., Lazio, T. J. W. 2002, (astro-ph/0207156)
- de Jager, O. C. 1991, *ApJ*, 378, 286
- Dewey, R. J., Taylor, J. H., Weisberg, J. M., Stokes, G. H. 1985, *ApJ*, 294, L25
- Geppert U., Küker M., Page D., 2004, *A&A*, 426, 267
- Gotthelf, E. V., Halpern, J. P., & Dodson, R. 2002, *ApJ*, 567, 125
- Halpern, J. P., & Wang, F. Y-H. 1997, *ApJ*, 477, 905
- Hobbs, G., Lyne, A. G., Kramer, M., Martin, C. E., Jordan, C. A. 2004, *MNRAS*, 353, 1311
- Kaminker, A. D., Haensel, P., & Yakovlev, D. G. 2001, *A&A*, 373, L17
- Lattimer, J. M., & Prakash, M. 2001, *ApJ*, 550, 426
- Mardia, K. V. 1972, *Statistics of Directional Data* (London: Academic)
- McGowan, K. E., Kennea, J. A., Zane, S., Córdova, F. A., Cropper, M., Ho, C., Sasseen, T., Vestrand, W. T. 2003, *ApJ*, 591, 380
- McGowan, K. E., Zane, S., Cropper, M., Kennea, J. A., Córdova, F. A., Ho, C., Sasseen, T., Vestrand, W. T. 2004, *ApJ*, 600, 343
- Nomoto, K., Tsuruta, S. 1987, *ApJ*, 312, 711
- Page, D., Lattimer, J.M., Prakash, M., Steiner, A.W. 2004, *ApJS*, 155, 623
- Possenti, A., Mereghetti, S., & Colpi, M. 1996, *A&A*, 313, 565

- Pavlov, G., et al. 1992, MNRAS, 253, 193
- Pavlov, G.G., Zavlin, V.E., Sanwal, D., et al., 2001, ApJ, 552, L129
- Pavlov, G. G., Zavlin, V. E., & Sanwal, D. 2002, in Proc. 270 WE-Heraeus Seminar, Neutron Stars, Pulsars, and Supernova Remnants, ed. W. Becker, H. Lesh, & J. Trümper (Garching bei München: MPI), 273
- Schaab, Ch., Sedrakian, A., Weber, F., Weigel, M. K. 1999, A&A, 346, 465
- Strüder, L., et al. 2001, A&A, 365, L18
- Yakovlev, D. G., Gnedin, O. Y., Kaminker, A.D., et al. 2002, (astro-ph/0306143)
- Turner, M. J. L., et al. 2001, A&A, 365, L27
- Zane, S., et al. 2002, MNRAS, 334, 345
- Zane, S., Turolla, R. 2005, Advances in Space Research, Vol. 35, Issue 6, p. 1162-1165, (astro-ph/0501094)
- Zavlin, V. E., et al. 1996, A&A, 315, 141
- Zavlin, V. E., Pavlov, G. G., & Trümper, J. 1998, A&A, 331, 821
- Zavlin, V. E., Trümper, J., & Pavlov, G. G. 1999, ApJ, 525, 959
- Zavlin, V. E., Pavlov, G. G., Sanwal, D., Manchester, R. N., Trümper, J., Halpern, J. P., Becker, W. 2002, ApJ, 569, 894

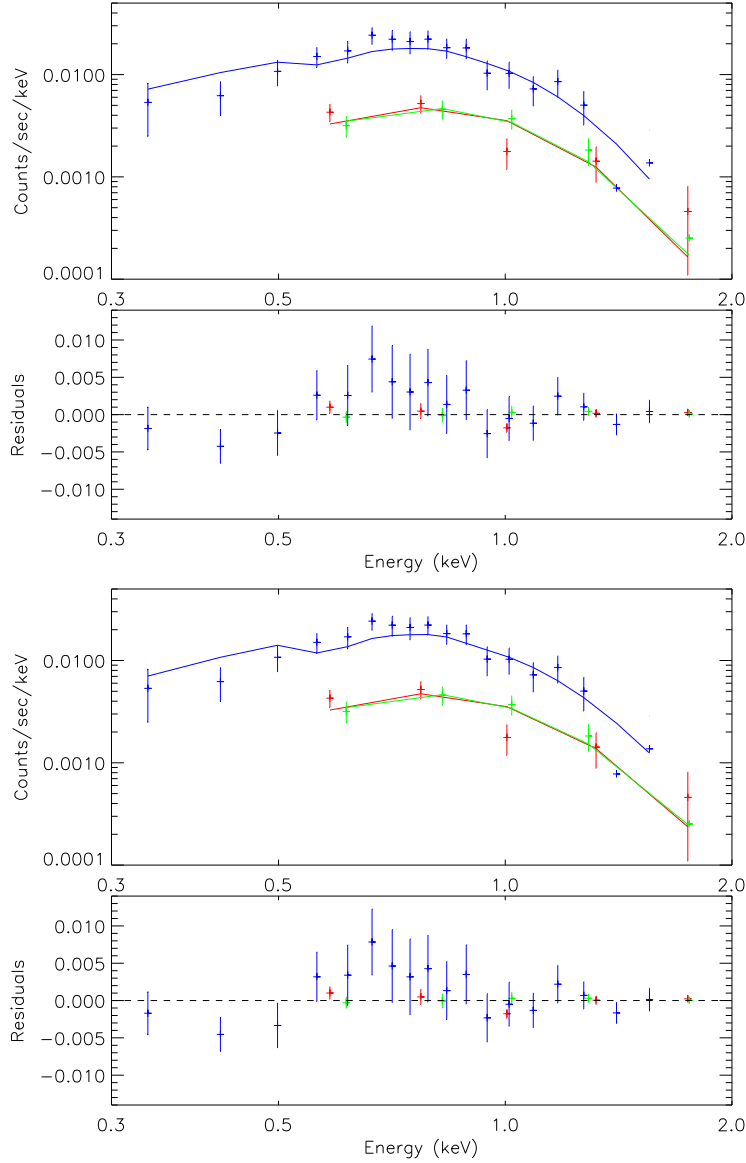


Fig. 1.— *XMM-Newton* PN and MOS spectra of the X-ray emission detected from PSR B2334+61. First panel: data (crosses) and best-fit blackbody model (solid line) for the parameters given in Table 1. Second panel: Difference between the data and the blackbody model. Third panel: data (crosses) and best-fit magnetized, pure H, atmospheric model (solid line) for the parameters given in Table 1 (NSA^b). Fourth panel: Difference between the data and the atmospheric model. In the electronic edition the PN, MOS1 and MOS2 data points, and best fit model where appropriate, are colored blue, red and green, respectively.

Table 1. Spectral fits to the X-ray emission from PSR B2334+61

Model	N_H (10^{22} cm $^{-2}$)	Γ	T/T_{eff}^∞ (10^6 K)	χ_ν^2/ν	F_X (erg cm $^{-2}$ s $^{-1}$)
PL	$0.90^{+0.09}_{-0.24}$	$8.47^{+1.53}_{-1.85}$...	38/25 = 1.5	$(6.37^{+26.06}_{-5.41}) \times 10^{-11}$
BB	$0.26^{+0.26}_{-0.05}$...	$1.62^{+0.23}_{-0.23}$	27/25 = 1.1	$(9.17^{+0.60}_{-0.86}) \times 10^{-14}$
BB+PL	$0.43^{+0.61}_{-0.17}$	$2.18^{+3.03}_{-1.44}$	$1.27^{+0.35}_{-0.58}$	24/23 = 1.0	$(3.06^{+1.27}_{-1.16}) \times 10^{-13}$
NSA ^a	$0.42^{+0.34}_{-0.04}$...	$0.58^{+0.13}_{-0.25}$	28/25 = 1.1	$(3.40^{+6.00}_{-3.26}) \times 10^{-13}$
NSA ^b	$0.33^{+0.41}_{-0.10}$...	$0.65^{+0.13}_{-0.34}$	31/25 = 1.2	$(1.68^{+0.09}_{-1.65}) \times 10^{-13}$
NSA ^b +PL	$0.26^{+0.73}_{-0.04}$	$9.44^{+0.55}_{-12.00}$	$0.76^{+0.09}_{-0.65}$	34/23 = 1.5	$(1.04^{+0.70}_{-1.04}) \times 10^{-13}$

Note. — Uncertainties are all at 90% confidence. Models used: “PL” indicates an absorbed power law with photon index Γ ; “BB” indicates an absorbed blackbody emitting at a temperature T ; “NSA” indicates an absorbed, magnetized, pure H atmospheric model with $B = 10^{13}$ G and effective temperature T_{eff}^∞ , as measured at Earth (Pavlov et al. 1992, Zavlin et al. 1996). For the NSA model we fixed the neutron star mass at $M_{NS} = 1.4M_\odot$, and the radius at 10 km (NSA^a) or 13 km (NSA^b). The last column is the unabsorbed flux in the 0.3 – 10 keV band.